Supplementary Information - Directed evolution of a bright variant of mCherry: Suppression of non-radiative decay by fluorescence lifetime selections

Srijit Mukherjee* [1, 2], Premashis Manna* [3], Sheng-Ting Hung [4], Felix Vietmeyer [1], Pia Friis [1], Amy E. Palmer [5, 6], and Ralph Jimenez [1, 2]

[1] JILA, University of Colorado, Boulder and National Institute of Standards and Technology, 440 UCB, Boulder, Colorado 80309, United States

[2] Department of Chemistry, University of Colorado, Boulder, 215 UCB, Boulder, Colorado 80309, United States

[3] Department of Chemistry, Massachusetts Institute of Technology, Cambridge, Massachusetts 02139, United States

[4] Department of Physics, National Sun Yat-sen University, Kaohsiung 80424, Taiwan

[5] Department of Biochemistry, University of Colorado at Boulder, 596 UCB, Boulder, Colorado 80309, United States

[6] BioFrontiers Institute, University of Colorado, Boulder, 596 UCB, Boulder, Colorado 80309, United States

* Equal contributions

Contents

List of Supplementary Figures

List of Supplementary Data Tables

Section 1. Mutagenesis Protocols

In order to develop RFP variants with higher brightness, we started with mCherry as a template. mCherry displays high photostability, excellent pH-resistance, fast maturation and a low cytotoxicity. However, mCherry is significantly dimmer than other recently developed RFPs, e.g. mRuby3,[1] mScarlet,[2] and FusionRed-MQV[3] in-part due to its lower quantum yield. To tackle this, we created several site-directed and random mutagenesis libraries and screened for higher excited state lifetime. Lifetime evolution was carried out using our microfluidic sorting platforms as previously reported. [4-6] We present a short discussion of the mutagenesis and library generation protocol below. Detailed protocols have been reported in our previous works.[3- 6]

- **Yeast and bacterial constructs for libraries and pure proteins**

Template construction: The original DNA templates for mCherry and other FPs were amplified with gene-specific primers and cloned into pDonr221 using Gateway recombination system (Life Technologies) and sequenced. The forward primer for each FP included a recombination recognition sequence (attB1), a Shine-Dalgarno sequence for prokaryotic expression, a BamH1 restriction endonuclease site, a Kozak sequence for mammalian expression and ~ 30 nucleotide sequence complementary to the FP. The reverse primer for each FP included ~ 30 nucleotides complementary to the FP, a stop codon, an EcoR1 restriction endonuclease site and an attB2 recombination recognition sequence. Using the Gateway recombination system, the LR reaction was performed to clone the FP into pYestDest52 vector (Life technologies). After sequences were confirmed the FP/pYestDest52 plasmids were used as template for library construction.

Error-prone libraries: GeneMorph II Random Mutagenesis kit (Agilent Cat No. 200550) was used to create the error-prone libraries. The kit protocol was followed with varying amounts of template DNA and cycles depending on the error rate. Like our work with FusionRed a typical error-rate is used that incorporates ~5 mutations (at the nucleotide level) per template. [3, 5] T7 and V5 universal primers (both located on pYesDest52 vector) were used for the amplification. After first round of PCR, the gel-extracted PCR product was used for a second round of PCR to create enough DNA for homologous recombination. After PCR purification the library DNA was isopropanol precipitated and eluted in a few µl of water.

Site directed libraries: QuikChange site-directed mutagenesis method was used to make point mutations or switch single amino acids using PfuTurboDNA polymerase and a Thermo cycler. PfuTurboDNA polymerase replicates both plasmid strands with high fidelity and without displacing the mutant oligonucleotide primers. The basic procedure utilizes a supercoiled double-stranded DNA (dsDNA) vector with the FP of interest and two synthetic oligonucleotide primers containing the desired mutation. The

oligonucleotide primers, each complementary to opposite strands of the vector, are extended during temperature cycling by PfuTurboDNA polymerase. Incorporation of the oligonucleotide primers generates a mutated plasmid containing staggered nicks. Following temperature cycling, the product is treated with DpnI. The DpnI endonuclease digests the parental DNA template and makes it possible to select for mutation-containing synthesized DNA. The nicked vector DNA containing the desired mutations is then transformed into *E. coli* (Top10). Libraries with multiple site-directed targets were created using SOE reaction (Splicing overlap extension). Primers were designed to introduce the desired mutations. The initial PCRs generate overlapping gene segments that are used as template DNA for another PCR to create a full-length product. The internal primers generate overlapping, complementary 30 ends on the intermediate segments and introduce the desired nucleotide changes for site-directed mutagenesis. Overlapping strands of these intermediate products hybridize at these 30 regions in a subsequent PCR and are extended to generate the full-length product amplified by flanking primers. The full-length product is gel-extracted and isopropanol-precipitated and eluted in a few µl water.

Electroporation: Fresh Competent yeast cells (*Saccaromyces cerevisiae* BY4741) were prepared prior to electroporation. Cells, DNA and cut pYestDest52 vector were combined and left on ice for 5 min. Electroporation conditions (Bio-Rad Gene Pulser Xcell): C = 25 µF, PC = 200-ohm, V = 1.5 kV (in 0.2 cm cuvettes). Cells were passed twice prior to expression. Mutants of were transferred to pBad-His vector for expression in *E. coli* and consequent Ni-NTA protein purification.

- **Mammalian Expression Constructs for FACS**

FPs were expressed as histone H2B fusion proteins in HeLa cells. Specifically, the mutants were PCR amplified from the pBad constructs with the upstream primer. Consequently, these were cut and ligated on piggyBac-H2B for expression in HeLa/U2OS cells. Cells were cultured in RPMI medium (Gibco Life Technologies) supplemented with penicillin/streptomycin (Gibco Life Technologies) and 10% heat-inactivated fetal bovine serum (Sigma-Aldrich) at 37°C with 5% CO_2 plus humidity. HeLa cells transiently transfected using the TransIT-LT1 reagent (Mirus, catalog #MIR2304) were prepared for FACS analysis after 48 hours.

Section 2. Mutagenesis and Directed Evolution of mCherry to mCherry-XL

We summarize our evolution efforts below and in Figures S1, S2, and S3.

- Site-directed mutagenesis on 16 (E/D/A/K/N/T/V), 17 (H/K/R) , 70 (K/R) , 99 (All 20), 143 (All 20), 161 (L/M/V/I/F), 163 (All 20 AA), 173 (All 20), 175 (All 20 AA) and 197 (All 20 AA) were triply- FACS enriched and revealed variations at positions 16, 17, 70, 99, 175 and 197.

- The positions 16, 17, 70, 99, and 197 were thus targeted and the triply FACS enriched library was addressed as the C-X (Cherry-X) library. Among these variants C9 and C12 were found to have longer lifetimes, but lower brightness in yeast than that of mCherry. In order to restore the brightness while maintaining their increased lifetimes, at first, we performed random mutagenesis. However, the random mutagenesis on C9 and C12 did not produce bright variants. (Figure S1)

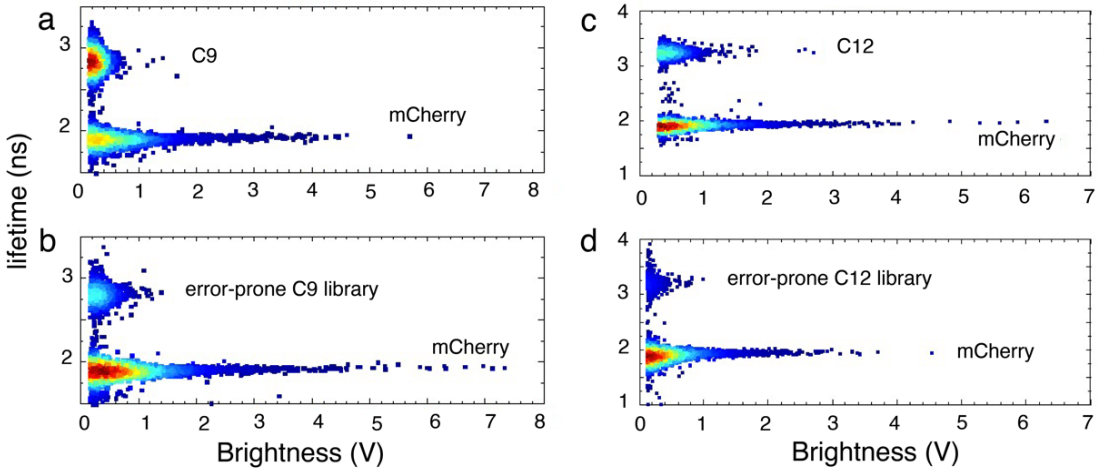

Figure S1: EP-PCR library of C9 and C12 variants. Microfluidic screening dot plots displaying lifetime and brightness (fluorescence signal in volts) of mCherry, C9, C12 and error-prone PCR libraries of C9 and C12. The pseudocolor indicates normalized cell counts with respect to the total number of screened/sorted cells at a certain value of brightness and lifetime on the plot – black indicating the highest and blue indicating the lowest. Each dot represents an individual yeast cell. It is evident from these plots that error-prone mutagenesis of C9 and C12 did not improve the lifetime and brightness of these variants. To collect these data, mCherry, the variants (C9, C12) and their EP-PCR libraries were expressed in yeast cells and screened on our microfluidic system with ~5000 cell counts. [3, 4]

- We, then performed targeted saturated mutagenesis on C9 and C12 at positions W143, I161 and Q163 based on bioinformatics guidance and sequence diversity of these amino-acid residues in

mFruit series of FPs.[7] We mixed the site-directed C9 and C12 libraries, (Figure 1; Main Text) which contained variants with high lifetime and brightness. This library was called C12-X. The C12-3 mutant was selected from this library, based on plate-based lifetime screening.

- An alternate evolution trajectory from the C12-X library led us to Site-Directed Clones (SDC), where we sorted the variants to enhance the populations with lifetime longer than 3.5 ns. We selected a few variants from this lifetime-enriched library and called them SDC variants. (e.g., variant SDC-5; QY~0.55, W143L, I161A, Q163L and I197R). The variants of the SDC-clones exhibit a green absorption peak – this evolution trajectory was consequently not pursued in the context of this study. Further analysis of this lineage can be found in Reference 8.[8]

- The C12-X library was subjected to two rounds of error-prone mutagenesis and selections for higher lifetime variants (with selection gate, lifetime> 3.7 ns) to generate the SLT (Selected-LifeTime) library. The SLT-11 mutant (mCherry N98S, R125H, F129L, Q137L, W143S, I161V, Q163Y, and I197R) was selected using plate-based lifetime screening in yeast from the lifetime enriched SLT library.

- A repeated error-prone effort on the SLT library yielded the EP-C12-X library without any improvement in lifetime or brightness. Consequently, we concluded that we arrived at the saturation of lifetime with the trajectory for directing the evolution of lifetime in mCherry.

- The octuple mutant SLT-11 had low protein yield in bacteria, consequently it could not be purified and fully characterized. Mutations at 98, 125, 129 and 137 were found to be external and far from the chromophore. Consequently, these positions were sequentially reverted to that of mCherry. Detailed investigations (single point reversions) revealed neither of these mutations had significant impacts on the excited state lifetime of the SLT-11 variant. We refer the reader to Section 3 of the SI and Reference 8 for further detailed investigations.[8] This led to the quadruple mutant that we address as mCherry-XL (mCherry W143S, I161V, Q163Y and I197R).

- Throughout the lifetime evolution a 561 nm excitation source (Coherent Genesis MX) and a 629/56 emission window (Semrock FF573-Di01- 25x36 / Semrock FF01- 629/56) provided additional selection pressures for selecting on a higher fluorescence brightness in yeast cells along with increased lifetime.[6]

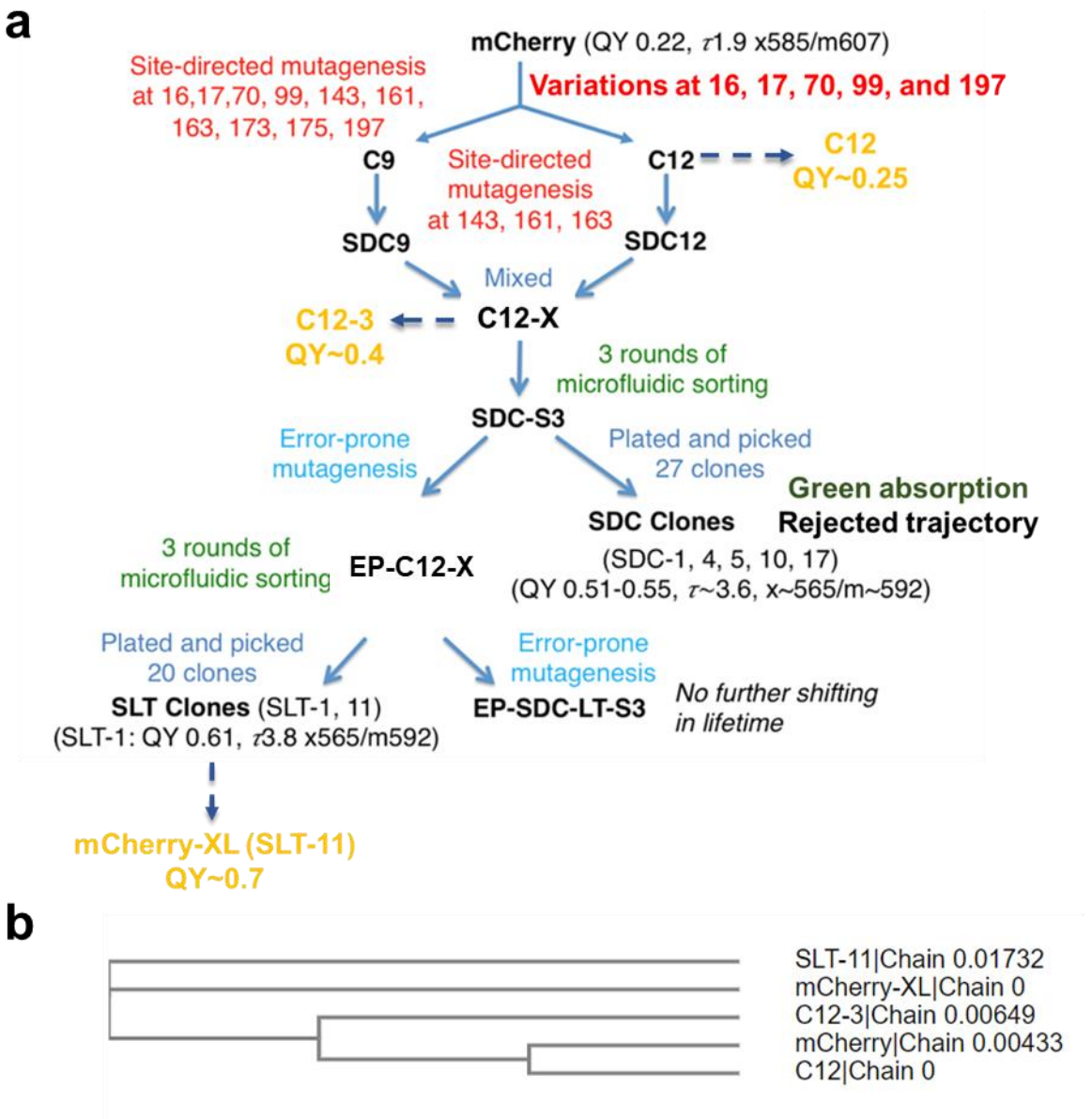

Figure S2: Summary of mutagenesis efforts on the mCherry family to achieve lifetime evolution. (a.) Evolution tree representative of phenotypic (photophysical) outcomes of the selections. The variants in gold were selected for characterization and study of co-evolution of other photophysical properties. **(b.)** A genetic representation of the evolution tree for the mutants relevant to this study.

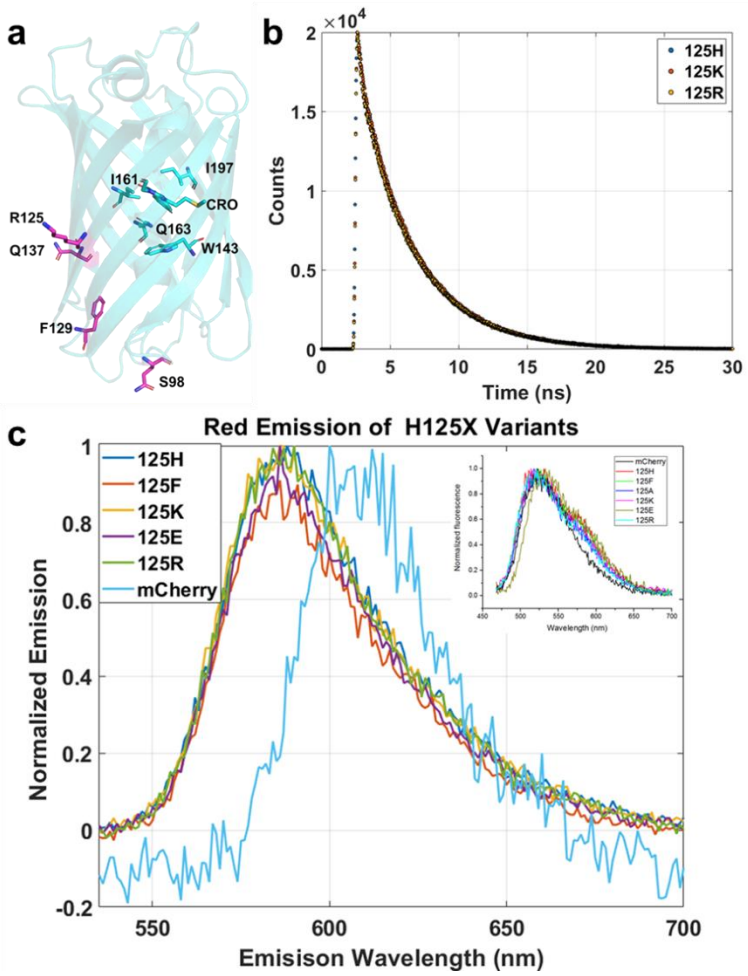

Figure S3: Role of spatially distant substitutions on the photophysical properties. (a.) mCherry's crystal structure (PDB ID: 2H5Q) suggests positions that do not impact the photophysics i.e., 98, 125, 129 and 137 are spatially distant (>15 Å) from the chromophore (denoted in purple). The chromophore and sidechains that perturb the photophysics of mCherry are denoted in cyan. Sidechains of 98, 125 and 137 also face out from the β-barrel, barring the exception of F129 which is located in the loop region with the sidechain facing inwards. The sidechain at 125 plays a role in the dimerization tendencies of DsRed derivatives like mCherry.[7] A positively charged sidechain e.g. R or K at 125 maintains the monomericity and does not change the photophysics of the FP. To elucidate this, we present; (**b.)** The similarity in fluorescence lifetime decay traces for the 125X variants of mCherry-XL measured using TCSPC. To test the monomericity, we present time-resolved fluorescence anisotropy measurements in Figure S9. Details for the other reversions are available in reference 8.[8] &, **(c.)** A minimal effect of substitutions at 125 on variants of mCherry-XL for the red emission with excitation at 520 nm. The inset indicates similarity in minimal green emission for these variants along with mCherry for excitation at 480 nm.

Section 3. Sequence Alignment of the RFP Variants

```
SLT-11|          EEDNMAIIKEFMRFKVHMEGSVNGHEFEIEGEGEGRPYEGTQTAKLKVTKGGPLPFAWDI 60
mCherry-XL|      EEDNMAIIKEFMRFKVHMEGSVNGHEFEIEGEGEGRPYEGTQTAKLKVTKGGPLPFAWDI
C12-3|           EEDNMAIIKEFMRFKVHMEGSVNGHEFEIEGEGEGRPYEGTQTAKLKVTKGGPLPFAWDI
C12|             EEDNMAIIKEFMRFKVHMEGSVNGHEFEIEGEGEGRPYEGTQTAKLKVTKGGPLPFAWDI
mCherry|         EEDNMAIIKEFMRFKVHMEGSVNGHEFEIEGEGEGRPYEGTQTAKLKVTKGGPLPFAWDI
                 ************************************************************

SLT-11|          LSPQFMYGSKAYVKHPADIPDYLKLSFPEGFKWERVMSFEDGGVVTVTQDSSLQDGEFIY 120
mCherry-XL|      LSPQFMYGSKAYVKHPADIPDYLKLSFPEGFKWERVMNFEDGGVVTVTQDSSLQDGEFIY
C12-3|           LSPQFMYGSKAYVKHPADIPDYLKLSFPEGFKWERVMNFEDGGVVTVTQDSSLQDGEFIY
C12|             LSPQFMYGSKAYVKHPADIPDYLKLSFPEGFKWERVMNFEDGGVVTVTQDSSLQDGEFIY
mCherry|         LSPQFMYGSKAYVKHPADIPDYLKLSFPEGFKWERVMNFEDGGVVTVTQDSSLQDGEFIY
                 ************************************.***********************

SLT-11|          KVKLHGTNLPSDGPVMLKKTMGSEASSERMYPEDGALKGEVKYRLKLKDGGHYDAEVKTT 180
mCherry-XL|      KVKLRGTNFPSDGPVMQKKTMGSEASSERMYPEDGALKGEVKYRLKLKDGGHYDAEVKTT
C12-3|           KVKLRGTNFPSDGPVMQKKTMGIEASSERMYPEDGALKGECKLRLKLKDGGHYDAEVKTT
C12|             KVKLRGTNFPSDGPVMQKKTMGWEASSERMYPEDGALKGEIKQRLKLKDGGHYDAEVKTT
mCherry|         KVKLRGTNFPSDGPVMQKKTMGWEASSERMYPEDGALKGEIKQRLKLKDGGHYDAEVKTT
                 ****:***:********.*****.*****************.* *****************

SLT-11|          YKAKKPVQLPGAYNVNRKLDITSHNEDYTIVEQYERAEGRHSTGGMDELYK 231
mCherry-XL|      YKAKKPVQLPGAYNVNRKLDITSHNEDYTIVEQYERAEGRHSTGGMDELYK
C12-3|           YKAKKPVQLPGAYNVNRKLDITSHNEDYTIVEQYERAEGRHSTGGMDELYK
C12|             YKAKKPVQLPGAYNVNRKLDITSHNEDYTIVEQYERAEGRHSTGGMDELYK
mCherry|         YKAKKPVQLPGAYNVNIKLDITSHNEDYTIVEQYERAEGRHSTGGMDELYK
                 ****************.*********************************
```

Table S1: Sequence alignment of the mCherry variants analyzed in this study. Variation in sequences have been highlighted with yellow/red. The positions highlighted in red show amino-acid substitutions that impact the photophysics of mCherry and its progeny, while the ones in yellow do not.

Section 4. Additional *in cellulo* assessments

Note: The version of mCherry-XL with the R125K substitution was used for cellular assessments.

a. Lifetime selection trajectory: Screening yeast cells for lifetime and cellular brightness

- **Screening on the microfluidic sorting device:** The proteins of interest, once selected out of the respective libraries were subjected to a round of microfluidic screening on the lifetime-sorter. Screenings were carried out at ~18-20 h post induction of FP in yeast cells with protocols used in the sorting experiments. Lifetime and brightness of biological triplicates of ~10,000 cells were recorded to report the screening data in yeast.

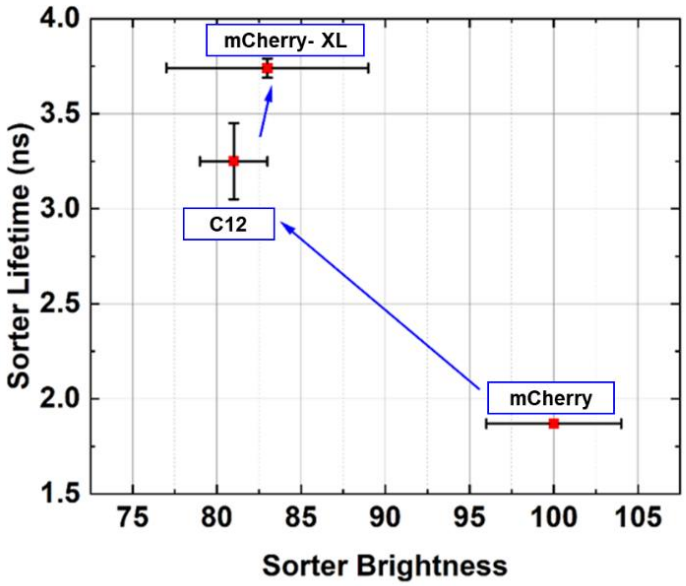

Figure S4. Lifetime & yeast-cell co-evolution trajectory. A screen of lifetime and brightness of single yeast cells on our microfluidic sorting devices [6] indicate the lifetime evolution trajectory from mCherry to mCherry-XL. Means and standard deviations of biological triplicates are reported. Despite a 2.5-fold higher lifetime, mCherry-XL is roughly 90% of the brightness of mCherry presumably due to slower chromophore maturation, low expression efficiency, etc in yeast. [5]

b. Brightness in mammalian cells

- **Flow cytometry:** The proteins of interest were fused to histone H2B and expressed in HeLa cells. Single-cell brightness was assessed by selecting single healthy cells based on forward and side-scattering photon counts on a BD FACSCelesta single cell analyzer after 48 h of transfection. Untransfected cells were used as a control to background subtract and analyze the fluorescence in the red and green channels. The samples were excited by a 561 nm laser line for collecting red fluorescence through the TRITC filter set (585/30 nm) and a 488 nm laser line for collecting through a GFP filter set (530/30 nm), to test for green fluorescence. mCherry-XL exhibited no green fluorescence like the progenitor mCherry.

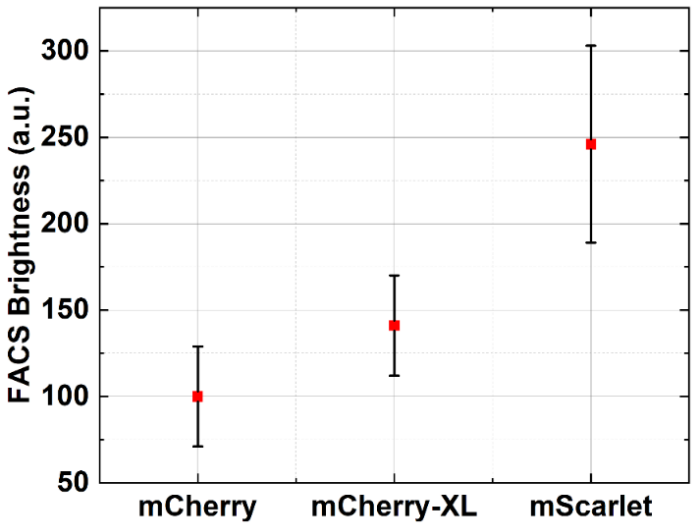

Figure S5: Cellular brightness in mammalian cells. A fluorescence activated cell sorting (FACS) based brightness assay in the H2B-FP construct in HeLa cells indicates mCherry-XL is 1.5-fold brighter than mCherry. FPs were cloned into a pcDNA3 plasmid C-terminal to H2B. Screenings were carried out at ~48 h post transfection. The error bars indicate the standard deviations from mean values of three biologically triplicate measurements. Each biological replicate measurement was comprised of a technical triplicate of 10000-20000 cells. The detailed methods for this assay have been discussed in a previous work. [3]

c. Photostability in bacteria

Photobleaching experiments and analysis were carried out in a similar fashion as our previous studies. [3, 10] We provide short descriptions to the sample preparation and data analysis below.

- **Sample Preparation and Experiment:** 2-3 fluorescent bacterial colonies from plates were washed with 500 µL imaging buffer (150 mM HEPES, 100 mM NaCl, pH 7.4) and centrifuged at 3000-5000 RPM for 60 s, and the washing buffer was removed. These cells were then resuspended in the same buffer to an OD in the range of 0.1 to 0.5 to get a cell density suitable for imaging. 10–20 µL of the cell mixture was added between a clean glass coverslip and slide. Imaging was carried on a widefield Olympus IX-73 inverted microscope system. Samples were excited by 560 nm continuous wave LED illumination (Lumencor). Time-lapse fluorescence bleaching measurements were collected through a 629/56 nm band-pass filter by a SCMOS camera (Andor Zyla) using an Olympus 20X objective. Irradiances ranging from 1–20 W/cm^2 were employed.

- **Data Analysis:** In brief, two pipelines in the CellProfiler suite (V2.2.0) was used to (a) identify bacteria on an imaging plane of uniform irradiance and (b) provide normalized intensity trajectories for the identified objects. The intensity trajectories were analyzed and fit to mono/bi/tri-exponential traces using a custom fitting program in MATLAB.

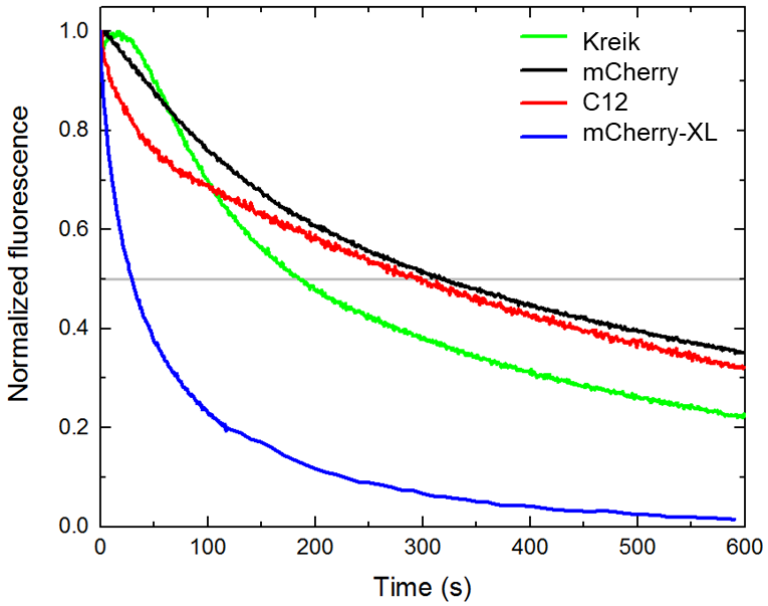

Figure S6: Photobleaching trends in *E. coli.* Bleaching profiles of mCherry, C12 and mCherry-XL are largely monoexponential and lack dark state conversion unlike FusionRed mutants investigated in our

previous studies. [3, 10] Data was collected at a continuous irradiation of ~10W/cm^2 (not excitation rate normalized). Kreik is a previously published mCherry variant selected out of photostability selections on a microfluidic platform. [9]

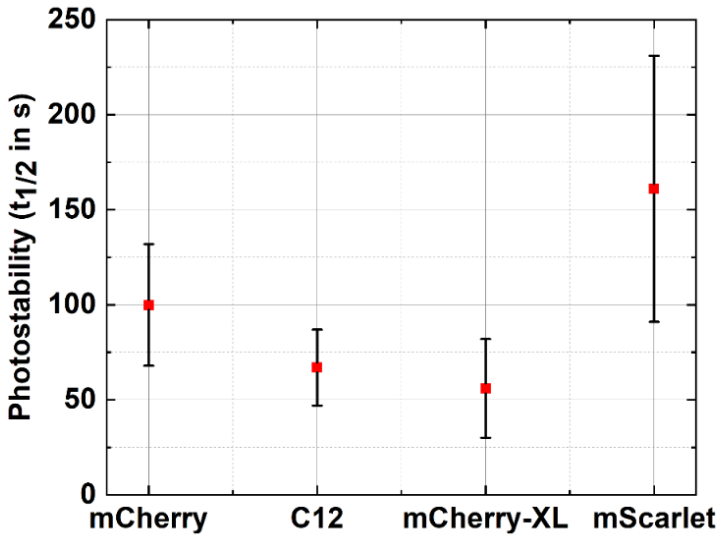

Figure S7: Comparing photostability under excitation rate normalized conditions in *E. coli.* Bacteria expressing RFPs of interest were photobleached under excitation normalized conditions using a 560 nm LED source at irradiances in the range of ~10 W/cm^2. These FPs showed a near mono-exponential photobleaching trace (Figure S6). [10] Therefore, the $t_{1/2}$ (s) is an accurate representation of photostability or the quantum yield of photobleaching under excitation rate normalized irradiation. [11] The expected trend of lower $t_{1/2}$ with increased excited state lifetime is also seen in this evolution study – in accordance with previous observations from the lifetime evolution efforts directed at FusionRed and mScarlet. [3, 10]

Section 5. Additional details for *in vitro* photophysical assessments

a. Spectral data of the variants

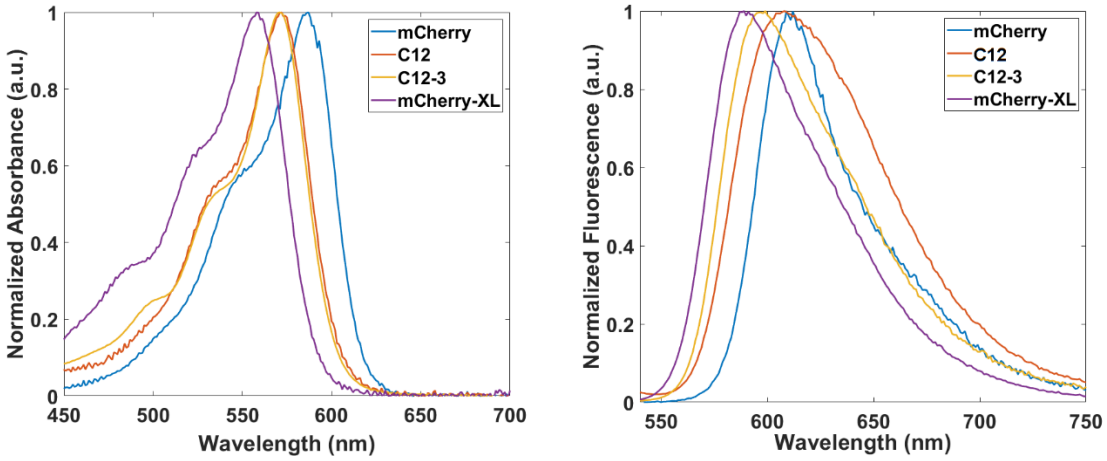

Figure S8: Normalized absorption and emission spectra. Normalized emission spectra **(right)** of the variants show blue-shifts from mCherry → mCherry-XL as it is observed in the absorption spectra **(left)**.

Table S2: Spectral properties of the RFP variants. Systematic blue shifts in absorption and emission peaks are observed with increments in fluorescence lifetimes. Integrated fluorescence, calculated from the normalized emission spectra of the variants correlates with the broadness of the emission. It is interesting to note that these variants have increased emission broadness and Stokes shift compared the parent mCherry.

RFP	λ_{abs} (nm)	λ_{em} (nm)	Stokes Shift (nm)	Int. Fluorescence
mCherry	587	609	22	66
C12	572	608	35	88
C12-3	571	599	28	77
mCherry-XL	558	589	31	79

b. Time-resolved fluorescence anisotropy

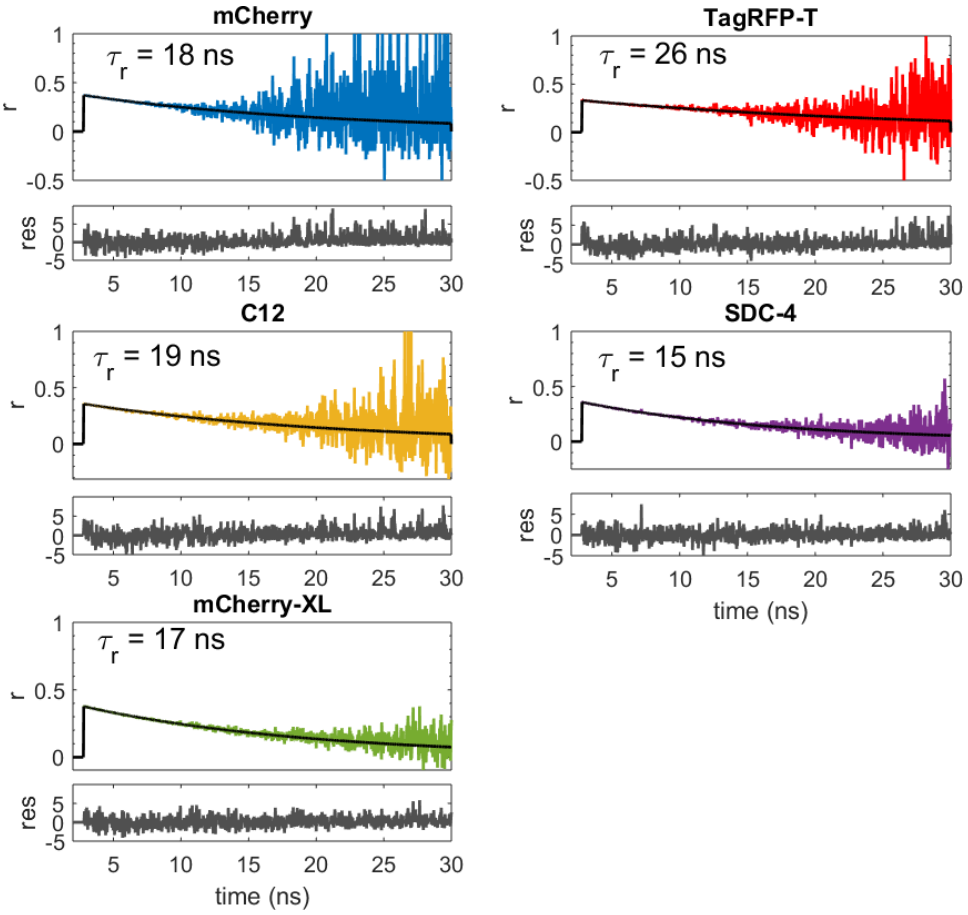

Figure S9: Fluorescence anisotropy decay and rotational time-constants (τ_r) of the variants. Anisotropy decay of the purified FPs were measured with our TCSPC instrument (Fluro Time 100, PicoQuant) as mentioned in the main text. 560 nm excitation and 5 MHz repetition rate were used. The rotational time-constant (τ_r) of each variant was obtained by fitting the fluorescence anisotropy decay with a single exponential function. All the variants were found to have τ_r similar to the parent mCherry, suggesting they likely retained *in vitro* monomeric character. TagRFP-T was characterized with slower τ_r, relative to the other variants. This is consistent with its reported *in cellulo* oligomerization tendencies. [3] The alternate evolution trajectory into SDC clones was not pursued due to a substantial green absorption peak. Details of the SDC variants are described elsewhere. [8]

c. Excited State Lifetime of the Variants

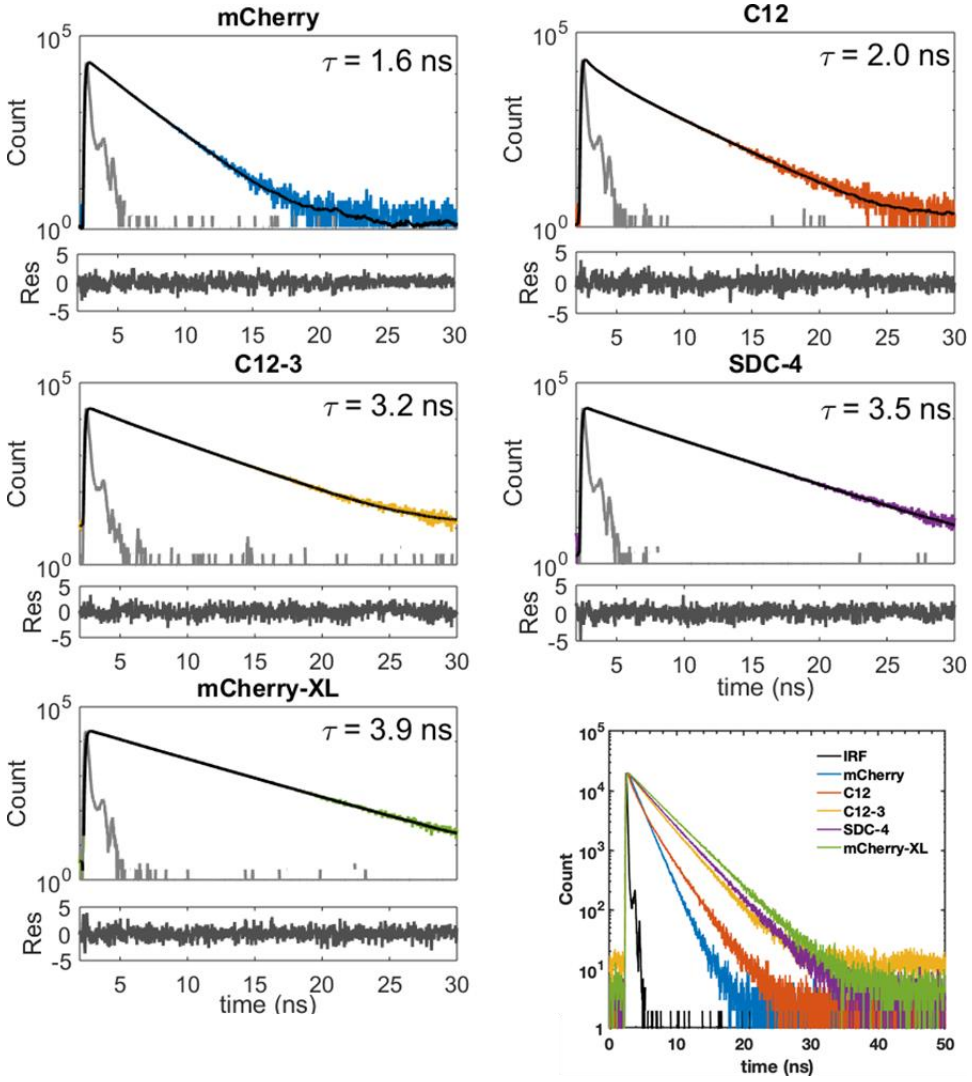

Figure S10: Fluorescence decay and the average lifetime (τ) of the variants. Excited state lifetimes are measured with our TCSPC system (Fluro Time 100, PicoQuant) using 560-nm laser excitation with a repetition rate of 5 MHz. Lifetime measurements were performed with purified proteins. The fluorescence transients of the FPs were fitted with iterative reconvolution with a bi or tri-exponential function (solid black line) and using the measured instrument response function (IRF) of the system (shown in grey). The values of lifetime were obtained by intensity weighted average of the fitted lifetime constants. [12] The alternate evolution trajectory into SDC clones was not pursued due to a substantial green absorption peak. Details of the SDC variants are described elsewhere. [8]

d. Measurement of fluorescence quantum yield

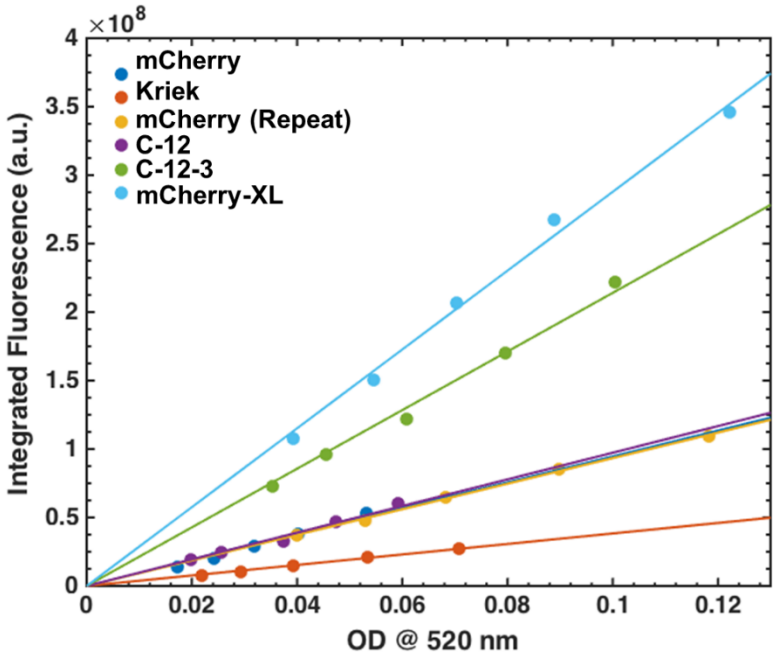

Figure S11: Fluorescence quantum yield (ϕ) of the variants. The quantum yield measurements were carried out by measuring the absorbance at 520 nm, and then collecting the integrated fluorescence over the entire red emission band (range 535-800 nm) across a step-dilution series. [3] A higher slope indicates a higher quantum yield, with mCherry (ϕ = 0.22) and Cresyl Violet in EtOH (ϕ = 0.54; data not shown) were used as references. [3]

e. Estimation of the extinction coefficient

- The values of peak extinction coefficient (ε_{max}) were determined using a ratiometric method as in our previous reports. [3] To measure the ε_{max}, the following protocol was used:
- Sample 1: Blank A - 900 µL of Tris-HCl buffer (pH 7.4). An absorption spectrum was recorded in the 250-750 nm range.
- Sample 2: Blank B - 900 µL of Tris-HCl buffer (pH 7.4) + 100 µL of 10 M NaOH (pH ~ 14). An absorption spectrum was recorded in the 250-750 nm range.
- Sample 3: 900 µL of Tris-HCl buffer (pH 7.4) + a few µL of concentrated purified protein sample was added to adjust the absorbance to a value of OD ~ 0.1. An absorption spectrum was recorded in the 250-750 nm range.
- Sample 4: 100 µL of 10 M NaOH was added to this solution. An absorption spectrum was recorded in the 250-750 nm range.
- In each case a 1 cm path length quartz cuvette was used.
- The ratiometric relationship provided below was used to calculate the value of the peak extinction coefficient. Three independent measurements were performed. Table 1 in the main text represents the value of the mean and the standard deviation errors.
- $$\epsilon_{max\text{RFP}} = \frac{\text{Abs}_{\text{max RFP}}}{\left(\frac{\text{Abs}_{380\text{ nm}}}{\epsilon_{380\text{ nm}}}\right)+\left(\frac{\text{Abs}_{450\text{ nm}}}{\epsilon_{450\text{ nm}}}\right)}$$
- Unlike members of the FusionRed family, [3] mCherry variants hydrolyze with a single product of denaturation, with an absorbance peak centered at 450 nm.

Section 6. Variation of the radiative rate constant

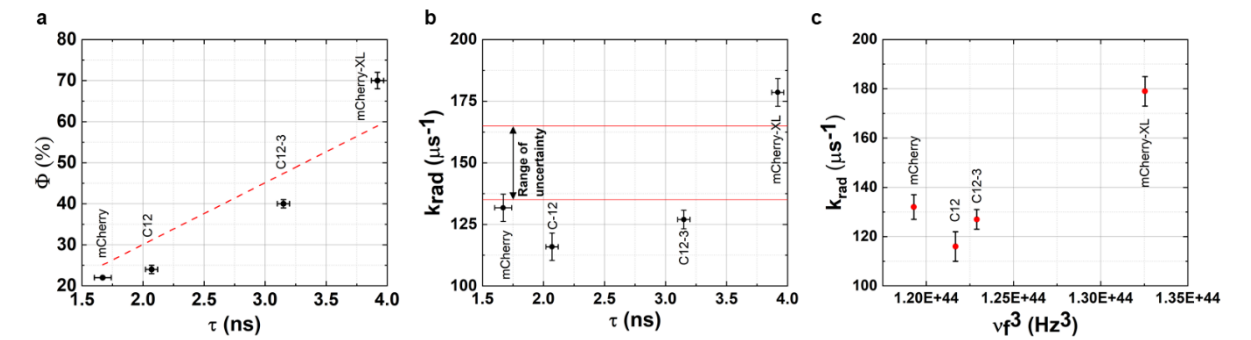

Figure S12: Analysis of the radiative rate constants for mCherry variants. **(a.)** A linear fit of the fluorescence quantum yield with the fluorescence lifetime indicates a good fit (R^2_{adj}~0.95). The slope of the linear fit (150 ± 14 μs^{-1}) is indicative of the average radiative rate constant. **(b.)** Values of calculated radiative rate constant with the fluorescence lifetime. The calculated values of the radiative rate constant lie outside the estimates provided by the average radiative rate (provided by the range of uncertainty calculated from the linear fit in panel a. on the figure). **(c.)** Values of calculated radiative rate constant with the cubed value of the peak fluorescence frequency. The calculated values of the radiative rate constants do not have a linear response with the cubed-value of the fluorescence frequency, thereby suggesting the change in the radiative rate constant is possibly due to multiple inter- or non-interconverting chromophores. This observation is further bolstered by multiexponential fluorescence lifetime decays. [11]

Section 7. Modelling non-radiative rate in the Englman-Jortner Low Temperature/Weak Coupling limit

A fit of the total non-radiative rate with the energy gap (or the 0-0 energy) shows a poor agreement with an Arrhenius type exponential decay. (Figure S13) This observation prompts investigating other models that incorporate the role of excited state reorganization along with the energy gap, such as the Englman-Jortner model for radiationless decay in large organic molecules. Details of this model and its treatment in FP systems can be found in ref # 11.[11]

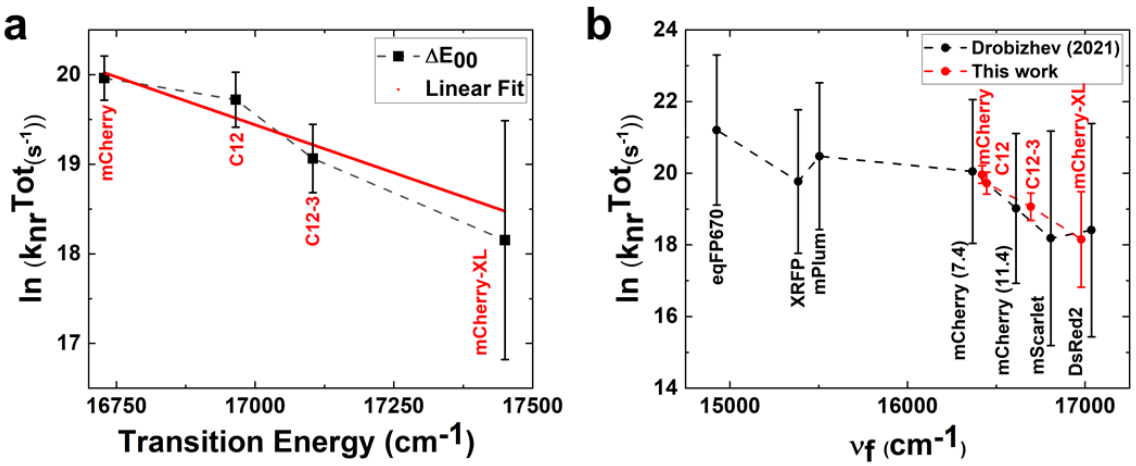

Figure S13: Fit of the total non-radiative rate constant with the energy gap. (a.) A linear fit (red line) of the logarithmic values of non-radiative rate (black squares) with the energy gap indicates a low-quality fit (R^2_{adj}~0.79). **(b.)** A comparison of non-radiative rate versus the fluorescence frequency for the variants investigated in this study with the analysis performed by the recent work of Drobizhev *et. al.* (2021). [13] The variants generated in this study display trends similar to what was investigated by Drobizhev et. *al* for a subset of unrelated RFPs. Error-bars reported are the percentage errors.

The shapes of absorption and fluorescence spectra for FPs of this family (Figure S8), indicate that the Huang-Rhys factor is < 1 because the 0-0 transition is more pronounced than the 0-1 vibronic shoulder. Additionally, the 0-0 transition energy >> Stokes-shift, and assuming these FPs lack any excited state photochemistry or excited state proton-transfer encourages the treatment of the non-radiative rate with a model where two electronic potential energy manifolds couple weakly. Therefore, we utilize the treatment of excited state vibrational relaxation from the low temperature weak/coupling case of the Englman-Jortner formalism. We now proceed to the estimation of the excited state reorganization energy.

a. Estimation of reorganization energy

The reorganization energy was estimated using the model provided by Jordanides *et. al.* [14] This method can provide an accurate representation for the reorganization energy for species that do not exhibit Gaussian absorption and fluorescence spectra (Figure S14). For species that do exhibit near Gaussian absorption and emission spectra a traditional method of estimating the reorganization energy from the Stokes-shift (λ_{SS}) can be used,[15]

$$\lambda_{SS} = 0.5\ (\max[\sigma_{abs}(\omega)] - \max[\sigma_{fl}(\omega)]), \qquad \text{Eq. S1}$$

Where $\sigma_{abs}(\omega)$ and $\sigma_{fl}(\omega)$ are the absorbance and fluorescence spectral lineshape functions in the frequency domain.

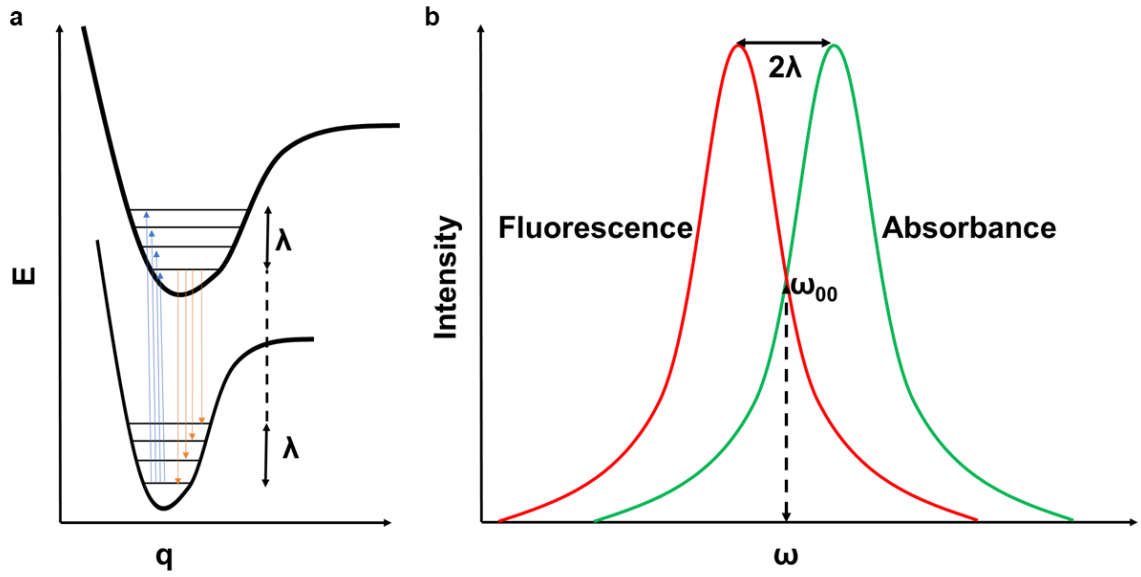

Figure S14: Schematic representations of relevant observables (a.) A two state potential energy surface indicating the visual depiction of the excited state reorganization energy. **(b.)** Representative Gaussian absorbance and fluorescence spectra with a 0-0 transition where the reorganization energy is exactly equal to half the Stokes Shift.

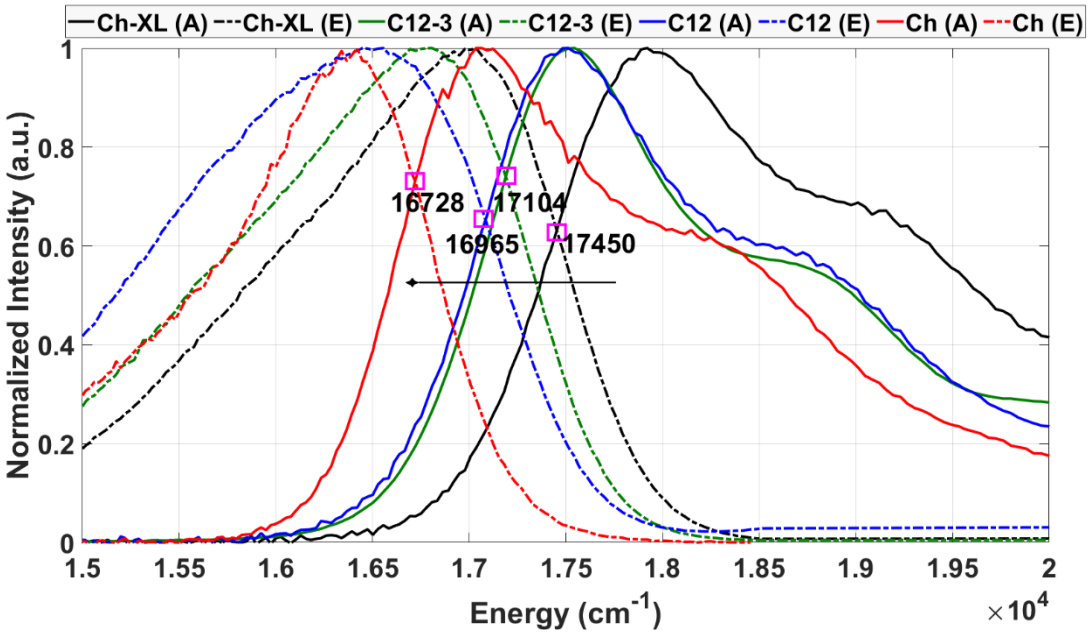

Figure S15: Absorbance and fluorescence spectra represented on the wavenumber scale. The spectra were scaled, also considering the nonlinear transformation of the wavelength scale to the wavenumber scale. [16] The pink boxes highlight the 00-transition energy and the arrow indicates the decrease in the energy gap of the transition.

However as shown in Figure S15, the presence of strong vibronic sidebands in the spectra for these FPs indicates deviation from Gaussian behavior. The model by Jordanides *et. al* provides a means of estimating the reorganization energy when this deviation from Gaussian behavior is observed. The only assumption of this model is that the polarization fluctuations of the dielectric medium follow Gaussian statistics (or the medium follows linear response). [14] The reorganization energy is calculated from the normalized difference of the first moment between the absorption and fluorescence spectra around the transition energy (ω_{00}). With this approach we arrive at the following expression for the reorganization energy:

$$\lambda_{SM} = \frac{\int d\omega\, \sigma_{\mathrm{abs}}(\omega-\omega_{00}) - \sigma_{\mathrm{fl}}(\omega-\omega_{00})\,(\omega-\omega_{00})}{\int d\omega\, \sigma_{\mathrm{abs}}(\omega-\omega_{00}) + \sigma_{\mathrm{fl}}(\omega-\omega_{00})}, \qquad \text{Eq. S2}$$

Using this method to calculate the reorganization energy, we arrive at significantly higher reorganization energy estimates. In reference 14 the reorganization energy of Eosin in water was estimated as 359 cm^{-1} using half the value of Stokes shift and 877 cm^{-1} and utilizing the spectral moments. We estimated values for EosinY in ethanol and observe similar trends with the reorganization energy from the Stokes-shift being 317 cm^{-1} and 706 cm^{-1} using the spectral moments. It should be noted that the tail ends of the absorption and emission spectrum must be carefully baseline-corrected to ensure accurate integration over the areas of

the sum and the difference spectrum. Poor baseline correction can result in erroneous values of the reorganization energy.

We performed this analysis for the RFP variants and observe that the spectral moments consistently provide larger estimates of reorganization energy than the Stokes-shift but the trends are consistent with both approaches (Table 3 and Figure 2, Main text). In both models, mCherry displays the lowest reorganization energy in this series of variants.

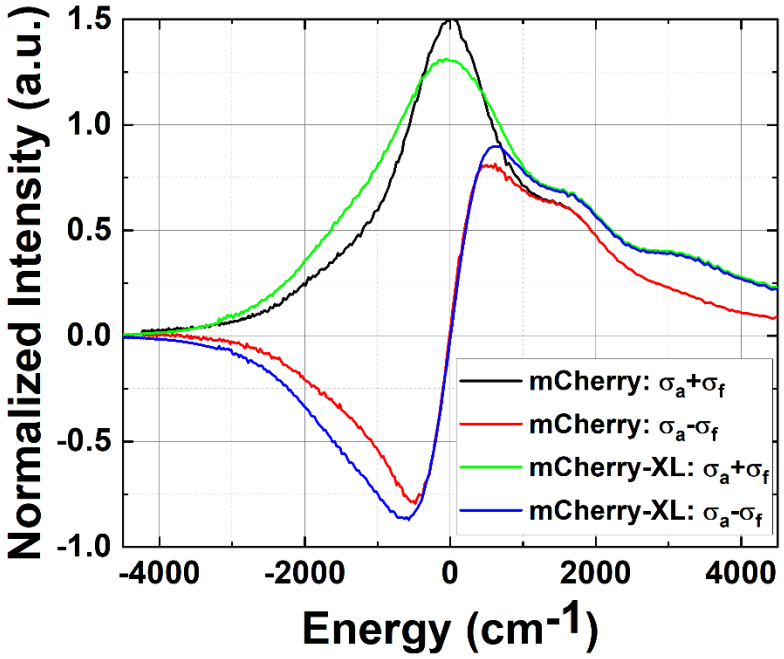

Figure S16: The numerator and denominator functions for in the Eq S2. The plots indicate the expected odd and even function behavior for mCherry and mCherry-XL respectively about $\omega - \omega_{00}$.

b. Validity of similar coupling constants for Herzberg-Teller coupling

In our analysis of non-radiative rates, we assume that the entire non-radiative rate in mCherry-XL derives from the values estimated from the Englman-Jortner approach. We then utilize this value, the energy gap, and the reorganization energy to estimate the coupling constant in the pre-exponent. Though the pre-exponent exhibits a very minor dependence on the overall non-radiative rate (as described in the original work of Englman and Jortner), it is important to provide a quantitative assessment for this assumption. These FPs exhibit a strong vibronic progression for the 0-1 vibronic transition in their absorption spectra (Figure S8). Therefore, to identify the strength of intensity borrowing of the 0-1 band from the 0-0 band, we fit the bands to two Gaussian functions and analyze their energy difference and the relative intensities. The energy difference can also be calculated using the second derivatives of the absorption spectra that reveal peak positions of these vibronic progressions. Using the spectral derivative method Lin *et. al.* arrived at a value of 1340 ± 40 cm^{-1} for the bond-length alteration (BLA) mode of the GFP chromophore. In our analysis (results are presented in Table S3), we found this difference to be a value of 966 ± 45 cm^{-1}, which can indicate a weaker BLA mode for the extended RFP chromophore system. [17]

Table S3: Difference in energies of the peaks of the 0-0 and 0-1 vibronic bands and the relative intensities.

FP	ΔE_{01}- ΔE_{00} (cm^{-1})	I_{00}/ I_{01}
mCherry	1008	2.05
C-12	924	2.31
C-12-3	930	2.17
mCherry-XL	1003	2.42

The minor (~10%) variation in the energy and the relative intensities provide quantitative validity to the assumption of a fixed Herzberg-Teller coupling constant for the RFP family.

References

1. Bajar, B. T.; Wang, E. S.; Lam, A. J.; Kim, B. B.; Jacobs, C. L.; Howe, E. S.; Davidson, M. W.; Lin, M. Z.; Chu, J. Improving Brightness and Photostability of Green and Red Fluorescent Proteins for Live Cell Imaging and FRET Reporting. Sci. Rep. **2016**, 6 (1), 20889. https://doi.org/10.1038/srep20889.

2. Bindels, D. S.; Haarbosch, L.; Van Weeren, L.; Postma, M.; Wiese, K. E.; Mastop, M.; Aumonier, S.; Gotthard, G.; Royant, A.; Hink, M. A.; Gadella, T. W. J. MScarlet: A Bright Monomeric Red Fluorescent Protein for Cellular Imaging. Nat. Methods **2016**, 14 (1), 53–56. https://doi.org/10.1038/nmeth.4074.

3. Mukherjee, S.; Hung, S. T.; Douglas, N.; Manna, P.; Thomas, C.; Ekrem, A.; Palmer, A. E; Jimenez, R. Engineering of a Brighter Variant of the Fusionred Fluorescent Protein Using Lifetime Flow Cytometry and Structure-Guided Mutations. Biochemistry **2020**, 59 (39), 3669–3682. https://doi.org/10.1021/acs.biochem.0c00484.

4. Dean, K. M.; Davis, L. M.; Lubbeck, J. L.; Manna, P.; Friis, P.; Palmer, A. E.; Jimenez, R. High-Speed Multiparameter Photophysical Analyses of Fluorophore Libraries. Anal. Chem. **2015**, 87 (10), 5026–5030. https://doi.org/10.1021/acs.analchem.5b00607.

5. Manna, P.; Hung, S. T.; Mukherjee, S.; Friis, P.; Simpson, D. M.; Lo, M. N.; Palmer, A. E.; Jimenez, R. Directed Evolution of Excited State Lifetime and Brightness in FusionRed Using a Microfluidic Sorter. Integr. Biol. (United Kingdom) **2018**, 10 (9), 516–526. https://doi.org/10.1039/c8ib00103k.

6. Hung, S. T.; Mukherjee, S.; Jimenez, R. Enrichment of Rare Events Using a Multi-Parameter High Throughput Microfluidic Droplet Sorter. Lab Chip **2020**, 20 (4), 834–843. https://doi.org/10.1039/c9lc00790c.

7. Shaner, N. C.; Campbell, R. E.; Steinbach, P. A.; Giepmans, B. N. G.; Palmer, A. E.; Tsien, R. Y. Improved Monomeric Red, Orange and Yellow Fluorescent Proteins Derived from Discosoma Sp. Red Fluorescent Protein. Nat. Biotechnol. **2004**, 22 (12), 1567–1572. https://doi.org/10.1038/nbt1037.

8. Manna, P. Development and Characterization of Improved Red Fluorescent Protein Variants, University of Colorado at Boulder, Boulder, 2018. https://www.proquest.com/dissertations-theses/development-characterization-improved-red/docview/2009736212/se-2?accountid=14503

9. Dean, K. M.; Lubbeck, J. L.; Davis, L. M.; Regmi, C. K.; Chapagain, P. P.; Gerstman, B. S.; Jimenez, R.; Palmer, A. E. Microfluidics-Based Selection of Red-Fluorescent Proteins with Decreased Rates of Photobleaching. Integr. Biol. (United Kingdom) 2015, 7 (2), 263–273. https://doi.org/10.1039/c4ib00251b.

10. Mukherjee, S.; Thomas, C.; Wilson, R.; Simmerman, E.; Hung, S. T.; Jimenez, R. Characterizing Dark State Kinetics and Single Molecule Fluorescence of FusionRed and FusionRed-MQ at Low Irradiances. ChemRxiv 2022. This content is a preprint and has not been peer-reviewed. https://doi.org/10.26434/chemrxiv-2022-2dr03

11. Mukherjee, S.; Jimenez, R. Photophysical Engineering of Fluorescent Proteins: Accomplishments and Challenges of Physical Chemistry Strategies. J. Phys. Chem. B, **2022.** https://doi.org/10.1021/acs.jpcb.1c05629

12. Sillen, A.; Engelborghs, Y. The Correct Use of "Average" Fluorescence Parameters. *Photochem. Photobiol.* **1998**, *67* (5), 475–486. https://doi.org/https://doi.org/10.1111/j.1751-1097.1998.tb09082.x.

13. Drobizhev, M.; Molina, R. S.; Callis, P. R.; Scott, J. N.; Lambert, G. G.; Salih, A.; Shaner, N. C.; Hughes, T. E. Local Electric Field Controls Fluorescence Quantum Yield of Red and Far-Red Fluorescent Proteins. Front. Mol. Biosci. 2021, 8 (February), 1–21. https://doi.org/10.3389/fmolb.2021.633217.

14. Jordanides, X. J.; Lang, M. J.; Song, X.; Fleming, G. R. Solvation Dynamics in Protein Environments Studied by Photon Echo Spectroscopy. *J. Phys. Chem. B* **1999**, *103* (37), 7995–8005. https://doi.org/10.1021/jp9910993.

15. Mertz, E. L.; Tikhomirov, V. A.; Krishtalik, L. I. Stokes Shift as a Tool for Probing the Solvent Reorganization Energy. *J. Phys. Chem. A* **1997**, *101* (19), 3433–3442. https://doi.org/10.1021/jp963042b.

16. Mooney, J.; Kambhampati, P. Get the Basics Right: Jacobian Conversion of Wavelength and Energy Scales for Quantitative Analysis of Emission Spectra. J. Phys. Chem. Lett. 2013, 4 (19), 3316–3318. https://doi.org/10.1021/jz401508t.

17. Lin, C. Y.; Romei, M. G.; Oltrogge, L. M.; Mathews, I. I.; Boxer, S. G. Unified Model for Photophysical and Electro-Optical Properties of Green Fluorescent Proteins. J. Am. Chem. Soc. 2019, 141 (38), 15250–15265. https://doi.org/10.1021/jacs.9b07152.